

A Poincaré section for the general heavy rigid body

Sven Schmidt^{1,2}, Holger R. Dullin^{1,2}, Peter H. Richter²

¹ Department of Mathematical Sciences,
Loughborough University, LE11 3TU, UK
h.r.dullin@lboro.ac.uk

² Institut für Theoretische Physik,
Universität Bremen, D-28334 Bremen, Germany

March 3rd, 2008

Abstract

A general recipe is developed for the study of rigid body dynamics in terms of Poincaré surfaces of section. A section condition is chosen which captures every trajectory on a given energy surface. The possible topological types of the corresponding surfaces of section are determined, and their 1:1 projection to a conveniently defined torus is proposed for graphical rendering.

Key words: general heavy rigid body, Poincaré surface of section, Euler–Poisson equations, bifurcation diagram, PP torus

1 Introduction

The dynamics of a rigid body in a constant field of gravity, with one point held fixed, is in general non-integrable. The configuration space $\text{SO}(3)$ has three degrees of freedom, but except for the special cases of Euler, Lagrange, and Kovalevskaya, the system possesses only two integrals of motion: the energy $H = h$ and the angular momentum component in the direction of gravity, $L_z = l$. Liouville integrability would require a third integral, but this does not exist. The parameter space is essentially 4-dimensional: when lengths, times, and energies are properly scaled, there remain two freedoms for the principal moments of inertia $A = \text{diag}(A_1, A_2, A_3)$, and two for the location of the body's center of mass $\mathbf{r} = (r_1, r_2, r_3)$ relative to the fixed point. Within this 4-D set of parameters, the Euler case $\mathbf{r} = 0$ defines a 2-D subset (two freedoms in the moments of inertia), Lagrange's case a

1-D subset (one free ratio of the moments of inertia, no freedom for the direction of \mathbf{r}), and Kovalevskaya's case is a single point (no freedom in the moments of inertia nor in the direction of \mathbf{r} , provided the body-fixed frame of reference is properly chosen). This implies that the vast majority of rigid body systems exhibits some degree of chaotic motion which to this very day has largely remained unexplored.

The three degrees of freedom of configuration space $\text{SO}(3)$ may be reduced to effectively two in view of the S^1 -symmetry with respect to the axis of gravity. Thereby the configuration space reduces to the Poisson sphere S^2 , and the corresponding 4-D phase spaces $T_l^*S^2$ are labeled with the angular momentum constant l . The surfaces $\mathcal{E}_{h,l}^3$ of constant energy $H = h$ are manifolds in $T_l^*S^2$, except at values (h, l) where their topological character undergoes a bifurcation. The first step in the analysis of phase space structure is the identification of the topology of $\mathcal{E}_{h,l}^3$, and of its bifurcation scheme. This requires to study the energy-momentum map from phase space to the (h, l) -plane, and to determine its critical values. Already this first step is more difficult than one might think. It has been worked out for certain subsets of parameters [7, 10] but not for the entire 4-D family of rigid bodies. However, even though the bifurcation schemes have not been resolved for all cases, it is known that the connected components of $\mathcal{E}_{h,l}^3$ come only in four types [11]: sphere S^3 , direct product $S^1 \times S^2$, real projective space \mathbb{RP}^3 , or connected sum $(S^1 \times S^2) \# (S^1 \times S^2)$.

Once the energy surfaces $\mathcal{E}_{h,l}^3$ are given, the problem is to find how they are partitioned into regular and irregular types of motion, i. e., into invariant subsets of one, two or three dimensions (isolated periodic orbits, resonant or non-resonant tori, and chaotic regions, respectively). The most valuable tool for this kind of studies is the method of Poincaré sections. It requires the identification of a 2-D surface of section $\mathcal{P}_{h,l}^2 \subset \mathcal{E}_{h,l}^3$ which intersects all possible trajectories. Finding such a global Poincaré section is a non-trivial matter. It is in general not possible to choose a surface which intersects all trajectories *transversally* [2]. However, it is possible to find a surface (or a set of disjoint surfaces) which is *complete* in the sense that every orbit intersects – or at least touches – it repeatedly. A constructive procedure to obtain such section conditions was given in [5] and will be employed here.

The next question refers to the topology of the surfaces of section, and how the various types of $\mathcal{P}_{h,l}^2$ may be adequately represented in two-dimensional plots. This is the main concern of the present paper. We show that a single connected component of $\mathcal{P}_{h,l}^2$ may be either a sphere S^2 , a torus T^2 , or a 2-D manifold M_g^2 of genus $g = 2, 3$, or 4. A single kind of

graphical representation applies to all cases: the 1:1 projection to a torus constructed from two copies of a two-fold punctuated Poisson sphere. We call this the “PP-torus” $T_2^2(\gamma)$ and propose it as a convenient universal tool for investigations of the complex dynamics of rigid bodies. For example, it may be interesting to vary (h, l) for fixed parameters (A_1, A_2, A_3) and (r_1, r_2, r_3) , in order to obtain a complete survey of the phase space structure for a given rigid body. For the integrable Kovalevskaya top such a survey was presented in [9], but the new tool can be applied to any choice of parameters. Alternatively, one might want to vary parameters at fixed (h, l) , and to follow the fate of certain conspicuous features (like isolated periodic orbits, or major chaotic regions).

The paper is organized as follows. Section 2 recalls how the topology of energy surfaces is determined from the effective potential on the Poisson sphere. The new Poincaré section is introduced in Section 3 and compared to a proposal made earlier in [6]. Finally, Section 4 describes the topology of the surfaces of section $\mathcal{P}_{h,l}^2$ and their projection first to the Poisson sphere, then to the PP-torus constructed from it.

2 Topology of energy surfaces

The heavy rigid body on $T^*\text{SO}(3)$ is symmetric with respect to rotation about the axis of gravity. Reduction by this symmetry gives the Euler-Poisson equations for the motion of a rigid body about a fixed point as seen in a co-moving frame,

$$\begin{aligned}\dot{\gamma} &= \{\gamma, H\} = \gamma \times \omega \\ \dot{\mathbf{l}} &= \{\mathbf{l}, H\} = \mathbf{l} \times \omega - mg\gamma \times \mathbf{r}.\end{aligned}\tag{1}$$

Here γ is the unit vector along the spatial z -axis (the axis of gravity), \mathbf{l} is the angular momentum vector, $\omega = A^{-1}\mathbf{l}$ the angular velocity vector, $A = \text{diag}(A_1, A_2, A_3)$ is the matrix of principal moments of inertia, and \mathbf{r} is the position of the center of mass in the body. The connection to Euler’s angles with respect to the z -axis is $(\gamma_1, \gamma_2, \gamma_3) = (\sin \psi \sin \vartheta, \cos \psi \sin \vartheta, \cos \vartheta)$; the angle φ of rotation about the z -axis is eliminated by the symmetry reduction. The remaining angles (ϑ, ψ) parameterize the Poisson sphere S^2 . The constants mg can be absorbed into \mathbf{r} and will be ignored from now on. These equations on the reduced phase space are Hamiltonian with respect to the Poisson bracket

$$\{F, G\} = \langle \nabla_\gamma F, \gamma \times \nabla_{\mathbf{l}} G \rangle + \langle \nabla_{\mathbf{l}} F, \gamma \times \nabla_\gamma G + \mathbf{l} \times \nabla_{\mathbf{l}} G \rangle\tag{2}$$

and Hamiltonian

$$H(\boldsymbol{\gamma}, \boldsymbol{l}) = \frac{1}{2} \langle \boldsymbol{l}, A^{-1} \boldsymbol{l} \rangle - \langle \boldsymbol{\gamma}, \mathbf{r} \rangle, \quad (3)$$

where $\langle \cdot, \cdot \rangle$ denotes the standard Euclidean scalar product in \mathbb{R}^3 . The bracket has two Casimirs¹,

$$I(\boldsymbol{\gamma}) = \langle \boldsymbol{\gamma}, \boldsymbol{\gamma} \rangle = 1 \quad \text{and} \quad L_z(\boldsymbol{\gamma}, \boldsymbol{l}) = \langle \boldsymbol{\gamma}, \boldsymbol{l} \rangle = l. \quad (4)$$

Fixing the Casimirs to the values $I(\boldsymbol{\gamma}) = 1$ and $L_z(\boldsymbol{\gamma}, \boldsymbol{l}) = l$ defines the reduced phase space $T_l^*S^2$. Fixing, in addition, the energy $H = h$ defines the reduced energy surface $\mathcal{E}_{h,l}^3$. The effective (or amended) potential on S^2 is, see e.g. [9],

$$U_l(\boldsymbol{\gamma}) = \frac{l^2}{2\langle \boldsymbol{\gamma}, A\boldsymbol{\gamma} \rangle} - \langle \boldsymbol{\gamma}, \mathbf{r} \rangle. \quad (5)$$

The term proportional to l^2 (the kinetic energy of rotation about the axis of gravity) contains the moment of inertia $\langle \boldsymbol{\gamma}, A\boldsymbol{\gamma} \rangle$. The accessible region on S^2 for fixed energy h and angular momentum l is

$$\mathcal{U}_{h,l} = \{\boldsymbol{\gamma} : U_l(\boldsymbol{\gamma}) \leq h\} \quad (6)$$

The energy-Casimir map is given by

$$\begin{aligned} F : \mathbb{R}^6 &\longrightarrow \mathbb{R}^3(h, l, 1) \\ (\boldsymbol{\gamma}, \boldsymbol{l}) &\longmapsto ((H(\boldsymbol{\gamma}, \boldsymbol{l}), L_z(\boldsymbol{\gamma}, \boldsymbol{l}), I(\boldsymbol{\gamma})) \end{aligned} \quad (7)$$

Its critical points $(\boldsymbol{\gamma}, \boldsymbol{l}) : \text{rank } DF < 3$, are the relative equilibria², and their images under F are the critical values. Since the last component of the energy-Casimir map is constant, it suffices to consider the (h, l) energy-momentum plane as the image. The energy surface $\mathcal{E}_{h,l}^3$ is the preimage of the point (h, l) . The set of critical values is called the bifurcation diagram. For critical values the energy surface is not a smooth manifold, and the topology in general changes upon crossing critical values.

Instead of computing the rank of F , the equilibria of (1) can be computed directly. The relation between the two approaches is that the gradients of the Casimirs are in the kernel of the Poisson structure, and if $\text{rank } DF$ is lower than 3, the gradient of the Hamiltonian is zero or a linear combination of the gradients of the Casimirs. A third method to obtain the relative equilibria is to compute the critical points of the effective potential U_l . The

¹note that l does not denote the length of \boldsymbol{l} , but the value of its z -component $\langle \boldsymbol{\gamma}, \boldsymbol{l} \rangle$.

²see Arnold [1], Appendix 5C.

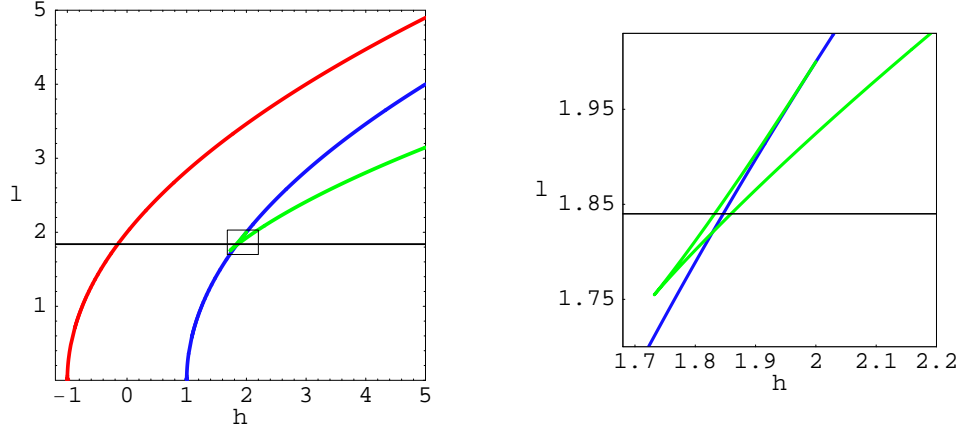


Figure 1: The bifurcation diagram showing critical values (h, l) of the energy-Casimir map F for the Kovalevskaya case $A = \text{diag}(2, 2, 1)$, $\mathbf{r} = (1, 0, 0)$. Right: Magnification of the rectangle shown on the left.

energy surface can be viewed as a singular circle bundle over the accessible region $\mathcal{U}_{h,l}$, see e. g. [2]. At critical points of U_l the topology of $\mathcal{U}_{h,l}$ changes, inducing a change in the topology of the energy surface. Thus a bifurcation diagram as shown in Fig. 1 can either be read as a statement about the existence of relative equilibria at the critical values shown, or as a statement about the topology of the reduced energy surface for the non-critical values.

For example [9], along the line $l = 1.84$ in Fig. 1, the topologies of the accessible regions $\mathcal{U}_{h,l}$ are, from left to right, empty set, disk, disk with two holes, disk with one hole, and all of S^2 . The transitions take place when crossing the lines of critical values in the bifurcation diagram. The corresponding topologies of the energy surface $\mathcal{E}_{h,l}^3$ are determined by the topology of the accessible region, see [2]. They are \emptyset , S^3 , $(S^1 \times S^2) \# (S^1 \times S^2)$, $S^1 \times S^2$, \mathbb{RP}^3 , again from left to right. More general cases of the bifurcation diagram have been discussed in [7, 11], see also [6].

It should be remembered that of the three Euler angles, only $\vartheta(t)$ and $\psi(t)$ appear in the Euler-Poisson equations; the angle $\varphi(t)$ must be determined by integration of [9]

$$\dot{\varphi} = \frac{l_1 \gamma_1 + l_2 \gamma_2}{2(\gamma_1^2 + \gamma_2^2)}. \quad (8)$$

Hence, relative equilibria $\boldsymbol{\gamma} = \text{const}$, $\mathbf{l} = \text{const}$ of the symmetry reduced system correspond to periodic motion of the full system.

3 Poincaré surface of section

For systems with two degrees of freedom and 3-dimensional compact energy surfaces, the relevant information about phase space structure (stability of periodic orbits, relative extent and entanglement of regular and chaotic motion) is contained in the 2-dimensional maps induced by the motion on suitably chosen Poincaré surfaces of section. This has become a standard tool from celestial mechanics to molecular dynamics, yet in the study of rigid bodies there have so far been only few applications [3, 4, 8]. However, as the Euler-Poisson equations describe a system with effectively two degrees of freedom (at given l), Poincaré sections are the ideal method to study the complexity of rigid body dynamics. In the following, we propose a variant which is at the same time general and easy to implement. We begin with a few general considerations.

3.1 General features of Poincaré sections

It would be nice to identify a two-dimensional submanifold $\mathcal{P}_{h,l}^2$ of the energy surface $\mathcal{E}_{h,l}^3$ in such a way that every orbit meets it repeatedly and transversally. As was shown in [5], *complete* sections can indeed be defined, i. e. sections which capture every single trajectory. However, globally transverse sections do not exist in general, for topological reasons [2]. Namely, when the surface of section $\mathcal{P}_{h,l}^2$ divides $\mathcal{E}_{h,l}^3$ into an “inner” and an “outer” part, trajectories that “come in” have to “go out” again, so that part of $\mathcal{P}_{h,l}^2$ is traversed by ingoing, another part by outgoing orbits. The boundary between the two is then a subset of $\mathcal{P}_{h,l}^2$ where the trajectories are tangent.

A complete surface of section $\mathcal{P}_{h,l}^2$ can be obtained with a recipe from [5]: given any smooth function W which maps the energy surface into a bounded set, define $S := \dot{W}$ and take $S(\gamma, l) = 0$ as section condition:

$$\mathcal{P}_{h,l}^2 := \{(\gamma, l) \in \mathcal{E}_{h,l}^3 : S(\gamma, l) = 0\} . \quad (9)$$

$\mathcal{P}_{h,l}^2$ is a smooth 2-dimensional manifold except when the map

$$\begin{aligned} P : \mathcal{E}_{h,l}^3 &\longrightarrow \mathbb{R}^4(h, l, 1, 0) \\ (\gamma, l) &\longmapsto (H(\gamma, l), L_z(\gamma, l), I(\gamma), S(\gamma, l)) \end{aligned} \quad (10)$$

has a critical point indicated by $\text{rank } DP(H, L_z, I, S) < 4$. Clearly the rank of P drops when the energy surface is not a smooth manifold, but there may be additional singular values.

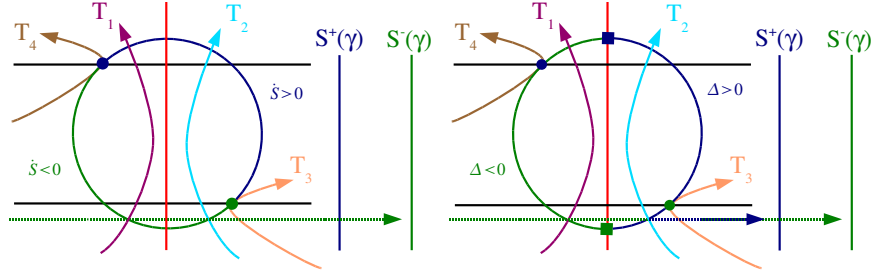


Figure 2: Schematic presentation of the Poincaré surface of section $\mathcal{P}_{h,l}^2$ (circle) with four trajectories two of which are tangent in the thick dots, and its projections onto two copies of the sphere $S^2(\gamma)$ (vertical bars). Left: S^\pm defined by the sign of \dot{S} (projections not invertible). Right: S^\pm defined by the sign of Δ .

The tangent set, if it exists, is given by those points on $\mathcal{P}_{h,l}^2$ for which $\dot{S} = 0$. Consider for example the Hamiltonian $H = \frac{1}{2}p_1^2 + \frac{1}{2}p_2^2 + V(q_1, q_2)$ and the section condition $S = q_2 = 0$.³ The surface of section is then given by $\mathcal{P}_h^2 = \{(q_1, p_1, p_2) : \frac{1}{2}p_1^2 + \frac{1}{2}p_2^2 + V(q_1, 0) = h\}$. Its usual representation is in terms of its projection to the (q_1, p_1) -plane which is a 2:1-map. To make it unique, only the part $\dot{q}_2 > 0$ is considered; the part $\dot{q}_2 < 0$ is ignored because the two parts are related by time reversal and contain no independent information. The line of tangency $\dot{S} = \dot{q}_2 = p_2 = 0$ lies in the projection plane and is in fact the boundary of the energetically accessible region $\{(q_1, p_1) : \frac{1}{2}p_1^2 + V(q_1, 0) \leq h\}$.

The situation is similar but somewhat more complicated in the case of rigid body dynamics. Assume we have a section condition $S(\gamma, \mathbf{l}) = 0$. The corresponding surface $\mathcal{P}_{h,l}^2 \subset \mathcal{E}_{h,l}^3$ “lives” in the 6-dimensional (γ, \mathbf{l}) -space, $\gamma \in S^2$ and $\mathbf{l} \in \mathbb{R}^3$. A convenient projection, as we shall see, maps it onto the Poisson sphere, $\pi : \mathcal{P}_{h,l}^2 \rightarrow S^2(\gamma)$. Here it is not generally true that the boundary of the projection coincides with the points of tangency. The situation is rather as shown schematically in the left part of Fig. 2. There $\mathcal{P}_{h,l}^2$ corresponds to the circle, and the bars to its right are meant to represent two copies of $S^2(\gamma)$. The four trajectories illustrate where $\mathcal{P}_{h,l}^2$ intersects incoming and outgoing orbits ($\dot{S} < 0$ and $\dot{S} > 0$, respectively). In this sketch, the line of tangency reduces to two points which may lie anywhere on the circle. Then, if $S^+(\gamma)$ were chosen to carry the projection

³This section condition is not of the form $S = \dot{W}$, hence it need not be complete; there may be orbits which never cross the line $q_2 = 0$ in the (q_1, q_2) -plane.

of the part where $\dot{S} > 0$, and likewise $S^-(\gamma)$ for $\dot{S} < 0$, these maps would obviously not be 1:1. In this setting, γ could not serve as a local coordinate on $\mathcal{P}_{h,l}^2$.

On the other hand, consider the right part of Fig. 2. There the circle representing $\mathcal{P}_{h,l}^2$ is divided by the two solid squares in such a way that the two projections to $S^\pm(\gamma)$ are indeed 1:1. A drawback of this welcome feature is that both projections contain incoming and outgoing intersections; the points of tangency no longer form the boundaries of the projections. But this turns out not to be serious. The important point is that the projections $S^\pm(\gamma)$ provide local coordinates on the two halves of $\mathcal{P}_{h,l}^2$. But how is this schematic picture to be implemented? It must be possible to uniquely determine the momenta \mathbf{l} on $\mathcal{P}_{h,l}^2$ from the coordinates γ . With $\mathcal{P}_{h,l}^2$ defined by $H = h$, $L_z = l$, and $S = 0$, the implicit function theorem guarantees that this can be done unless

$$\Delta(\gamma, \mathbf{l}) := \det \frac{\partial}{\partial \mathbf{l}}(H, L_z, S) = 0. \quad (11)$$

The relevant division of $\mathcal{P}_{h,l}^2$ into two parts is therefore given by the sets $\mathcal{P}_{h,l}^+ \subset \mathcal{P}_{h,l}^2 : \Delta > 0$ and $\mathcal{P}_{h,l}^- \subset \mathcal{P}_{h,l}^2 : \Delta < 0$ which project to $S^+(\gamma)$ and $S^-(\gamma)$ respectively. The condition (11) contains the definition of the dividing line on $\mathcal{P}_{h,l}^2$. It will be seen in (15) that there may exist other lines in $\mathcal{P}_{h,l}^2$ where $\Delta = 0$, but these project only to points in $S^2(\gamma)$.

Note that even when the system is symmetric under time reversal (which is not the case here, at fixed $l \neq 0$), it may not be sufficient to consider only one of the two projections. As can be seen in Fig. 3, orbits with intersection points close to tangency tend to have incoming and outgoing intersections with the same sign of Δ ; hence, in order to capture all orbits, both projections are needed.

3.2 The section condition

The first general section condition of the type $S = \dot{W}$ was proposed in [6] with $W = \langle \mathbf{l}, \mathbf{l} \rangle$. It was motivated by a study of the projections of the energy surfaces $\mathcal{E}_{h,l}^3$ to \mathbf{l} -space. There the preimages of the envelopes of these projections could be characterized by $S = 0$, or $\langle \mathbf{l}, \gamma \times \mathbf{r} \rangle = 0$, i. e. in terms of local extrema of the values of the total angular momentum. Clearly this section condition is the adequate choice when the envelopes in \mathbf{l} -space are used to represent the Poincaré surfaces of section; a number of beautiful examples have been worked out in this setting (Gashenenko, private communication). However, the complex topology of the corresponding surfaces $\mathcal{P}_{h,l}^2$

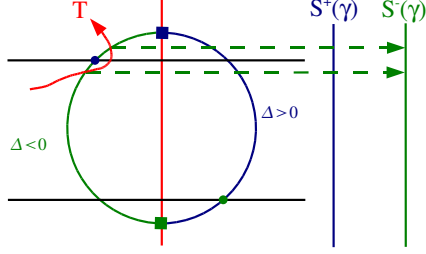


Figure 3: Only both copies of $S^2(\gamma)$ allow a complete characterization of the phase space structure since intersection points can be projected to one copy only.

(being manifolds of genus up to five and even higher) makes it hard to study them. Furthermore, the \mathbf{l} -envelopes are different for each point (h, l) , and difficult to parameterize, hence they do not lend themselves for extended investigations. An obvious way out of this last difficulty is to project the surfaces $\mathcal{P}_{h,l}^2$, defined by $W = \langle \mathbf{l}, \mathbf{l} \rangle$, to the Poisson sphere $S^2(\gamma)$. However, it turns out [6] that this produces artifacts in the projections which have no relevance in $\mathcal{P}_{h,l}^2$ itself: the condition $W = \langle \mathbf{l}, \mathbf{l} \rangle$ is well adapted for \mathbf{l} -space, not for γ -space.

Therefore we propose another choice:

$$W = \langle \gamma, \mathbf{r} \rangle \quad \Rightarrow \quad S(\gamma, \mathbf{l}) = \frac{dW}{dt} = \langle A^{-1} \mathbf{l}, \mathbf{r} \times \gamma \rangle = 0. \quad (12)$$

This is motivated by the behavior of the Lagrange top where \mathbf{r} lies on the body axis so that $\langle \gamma, \mathbf{r} \rangle \propto \cos \vartheta$. The angle ϑ oscillates between ϑ_{\min} and ϑ_{\max} which makes $\vartheta = 0$ a natural section condition. In addition, when successive points (ϑ_n, ψ_n) ($n = 0, 1, 2, \dots$) of the corresponding Poincaré map are plotted on $S^2(\gamma)$, a natural winding number may be read off in terms of the increments of ψ . The section condition (12) is an obvious generalization; it picks out extrema of the projection of the center of mass \mathbf{r} to the vertical direction. As we will show, the resulting surfaces of section $\mathcal{P}_{h,l}^2$ have genus only up to 4, and they have fewer bifurcations than those studied in [6]. Moreover, the projections $\pi(\mathcal{P}_{h,l}^2)$ onto the Poisson sphere coincide with the accessible region $\mathcal{U}_{h,l}$, and the condition $\Delta(\gamma, \mathbf{l}) = 0$ defines a line which projects to the boundary $\partial \mathcal{U}_{h,l}$. Finally, this projection is simple because generically it has exactly two preimages; the exceptions are $\gamma \in \partial \mathcal{U}_{h,l}$ which have only one preimage, and $\gamma \parallel \mathbf{r}$ where the preimage is a circle.

To prove these statements, we simultaneously solve the equations $H = h$, $L = l$ (which together define the energy surface $\mathcal{E}_{h,l}^3$) and $S = 0$; i. e., given

a point γ on the Poisson sphere, we determine the set of corresponding values \mathbf{l} such that $(\gamma, \mathbf{l}) \in \mathcal{P}_{h,l}^2$. The explicit calculation is given in the Appendix. There we excluded the possibility that γ and \mathbf{r} are collinear, $\mathbf{r} \times \gamma = 0$, so let us start here with this case: $\gamma = \pm \mathbf{r}/r =: \hat{\mathbf{r}}$. The condition $S = 0$ is then identically fulfilled and gives no restriction on \mathbf{l} . The condition $L_z = \langle \mathbf{l}, \gamma \rangle = l$ defines a plane in \mathbf{l} -space, and $H = h$ the ellipsoid $\langle \mathbf{l}, A^{-1}\mathbf{l} \rangle = 2(h + \langle \mathbf{r}, \gamma \rangle) = 2(h \pm r)$. Three cases are possible:

- (i) The intersection of plane and ellipsoid is a topological circle.
- (ii) They do not intersect at all.
- (iii) The plane is tangent to the ellipsoid in a point \mathbf{l}^* .

In the latter case the normal to the ellipsoid must be collinear with γ , i. e. $A^{-1}\mathbf{l}^* = \xi\gamma$ or $\mathbf{l}^* = \xi A\gamma$. From $\langle \mathbf{l}^*, \gamma \rangle = l$ we obtain $\xi = l/\langle \gamma, A\gamma \rangle$, hence the energy equation becomes

$$\frac{l^2}{\langle \gamma, A\gamma \rangle} = 2(h \pm r) \quad \Leftrightarrow \quad h = U_l(\gamma) = U_l(\pm \hat{\mathbf{r}}). \quad (13)$$

So in this case, $\gamma = \pm \hat{\mathbf{r}}$ lies on the boundary of the accessible region, $\gamma \in \partial\mathcal{U}_{h,l}$. In case (i), γ lies inside, in case (ii) outside. This will be relevant for the topology of $\mathcal{P}_{h,l}^2$, see next section.

Let us now consider γ which are not collinear with \mathbf{r} . We show in the Appendix that given γ , the preimages in $\mathcal{P}_{h,l}^2$ are the points (γ, \mathbf{l}) with

$$\mathbf{l} = l \frac{A\gamma}{\langle \gamma, A\gamma \rangle} \pm \mathbf{v} \sqrt{\frac{2(h - U_l(\gamma))}{\langle \mathbf{v}, A^{-1}\mathbf{v} \rangle}}, \quad (14)$$

where $\mathbf{v} = (A^{-1}(\mathbf{r} \times \gamma)) \times \gamma$. This tells us that for all γ with $U_l(\gamma) < h$, or γ from the interior of $\mathcal{U}_{h,l}$, there are exactly two preimages in $\mathcal{P}_{h,l}^2$. For γ on the boundary, $\gamma \in \partial\mathcal{P}_{h,l}^2$, the preimage is unique. No real \mathbf{l} exists for γ outside $\mathcal{U}_{h,l}$.

Computing the determinant $\Delta(\gamma, \mathbf{l})$ according to Eq. (11), we find

$$\Delta(\gamma, \mathbf{l}) = \langle A^{-1}\mathbf{l} \times \gamma, A^{-1}(\gamma \times \mathbf{r}) \rangle. \quad (15)$$

This is zero for $\gamma \in \partial\mathcal{U}_{h,l}$, where $A^{-1}\mathbf{l} \times \gamma = 0$, corroborating the assertions made in connection with the right panel of Fig. 2: the parts of $\mathcal{P}_{h,l}^2$ where $\Delta > 0$ and $\Delta < 0$ each project to the entire accessible region $\mathcal{U}_{h,l} \subseteq S^2(\gamma)$. (Note that $\mathcal{U}_{h,l}$, hence also $\mathcal{E}_{h,l}^3$ and $\mathcal{P}_{h,l}^2$, may consist of several disconnected

components.) The other possibility for Δ to become zero, $\boldsymbol{\gamma} \times \mathbf{r} = 0$, is of another kind; its projection to $S^2(\boldsymbol{\gamma})$ gives at most the two points $\boldsymbol{\gamma} = \pm \hat{\mathbf{r}}$. If they are inside $\mathcal{U}_{h,l}$, their preimages in $\mathcal{P}_{h,l}^2$ are circles, see case (i) above Eq. (13). The consequences are discussed in the next section.

The condition $\dot{S} = 0$ for tangency of trajectories with $\mathcal{P}_{h,l}^2$ is obtained from (12) by differentiation:

$$\dot{S} = \langle A^{-1}(\mathbf{l} \times A^{-1}\mathbf{l} - \boldsymbol{\gamma} \times \mathbf{r}), \mathbf{r} \times \boldsymbol{\gamma} \rangle + \langle A^{-1}\mathbf{l}, \mathbf{r} \times (\boldsymbol{\gamma} \times A^{-1}\mathbf{l}) \rangle = 0. \quad (16)$$

This must be considered together with (14). We do not attempt to derive an explicit expression for the projection of these lines to the Poisson sphere, but they will be shown in the graphical representations of the following sections.

4 Topology of $\mathcal{P}_{h,l}^2$ and its projections

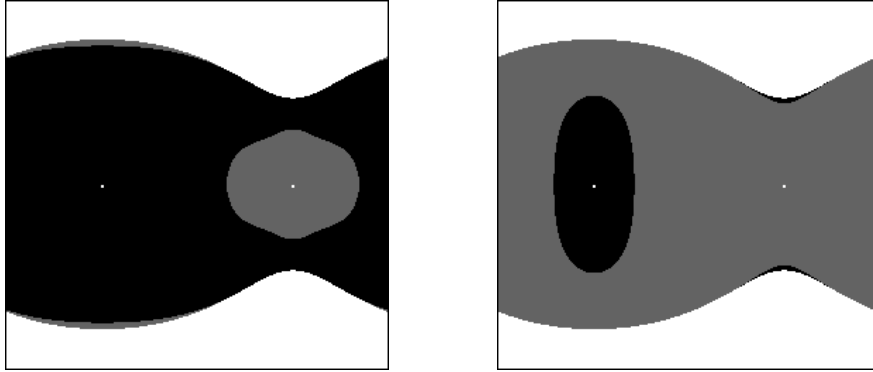


Figure 4: Projection of $\mathcal{P}_{h,l}^2$ onto the Poisson spheres $S^-(\boldsymbol{\gamma})$ (left) and $S^+(\boldsymbol{\gamma})$ (right). On the abscissa ψ goes from 0 to 2π , the ordinate ϑ varies from 0 (top) to π (bottom). $A = (2, 2, 1)$, $\mathbf{r} = (1, 0, 0)$, $h = 3.4$, $l = 2.87$.

Fig. 4 shows a typical projection of $\mathcal{P}_{h,l}^2$ to two copies $S^-(\boldsymbol{\gamma})$ (left) and $S^+(\boldsymbol{\gamma})$ (right) of the Poisson sphere, for $A = (2, 2, 1)$ and $\mathbf{r}(1, 0, 0)$. The coordinates of the two panels are $0 \leq \psi < 2\pi$ on the abscissa and $0 \leq \vartheta \leq \pi$ on the ordinate. The white regions at small and large ϑ are inaccessible with the given values of $h = 3.4$ and $l = 2.87$. The grey and black parts together are the accessible region $\mathcal{U}_{h,l}$ which has the topology of an annulus. In the black parts the trajectories are incoming, $\dot{S} < 0$, in the grey region they are

outgoing, $\dot{S} > 0$; the boundary between these regions is the set of tangency. If we were to record only incoming trajectories, only the black parts needed to be considered, but note it appears on both copies $S^\mp(\gamma)$.

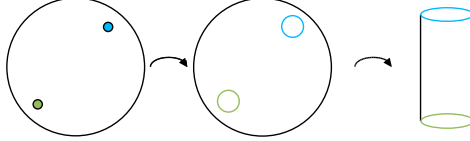


Figure 5: For a topologically more adequate representation of the preimages in $\mathcal{P}_{h,l}^2$ of the poles $\gamma = \pm \hat{\mathbf{r}}$, these poles are replaced by “polar circles” which turns the Poisson sphere into a cylinder.

The white dots at $(\vartheta, \psi) = (\pi/2, \pi/2)$ are the “north pole” $\gamma = \hat{\mathbf{r}}$, the white dots at $(\pi/2, 3\pi/2)$ are the “south pole” $\gamma = -\hat{\mathbf{r}}$. We know from the previous section that these points are special. When they are physically accessible as they are here, then their preimage in $\mathcal{P}_{h,l}^2$ is a circle (instead of a point as for all other γ). This suggests to represent $\mathcal{P}_{h,l}^2$ not in projection to a sphere but rather to a cylinder: punctuate $S^2(\gamma)$ at the poles and insert “polar circles” there, as illustrated schematically in Fig. 5. Instead of the two spheres S^\mp we then have two cylinders for the projections of $\mathcal{P}_{h,l}^-$ and $\mathcal{P}_{h,l}^+$. But notice that these two cylinders share the same circles at the poles, hence together they form a torus T^2 which we shall call the “PP-torus” $T_2^2(\gamma)$, the two P’s referring to Poisson and Poincaré, or to the two copies of the punctuated Poisson sphere, and the subscript 2 indicating that each γ is represented twice. We denote its two halves by T^- , T^+ , and remark that each carries one copy of $\mathcal{U}_{h,l}$. $\mathcal{P}_{h,l}^-$ and $\mathcal{P}_{h,l}^+$, respectively, project 1:1 to interior points of the two $\mathcal{U}_{h,l}$, and their boundary, defined by $\Delta(\gamma, \mathbf{l}) = 0$, projects to $\partial\mathcal{U}_{h,l}$. Thus, if we identify the two copies of $\partial\mathcal{U}_{h,l}$ on T^- and T^+ , we obtain a 1:1 map $\mathcal{P}_{h,l}^2 \rightarrow T_2^2(\gamma)$ which preserves the topology.

The graphical implementation of this idea is automatically achieved if we first transform to new polar coordinates (ϑ', ψ') where $\gamma = \hat{\mathbf{r}}$ is taken as polar axis instead of $\gamma = (0, 0, 1)$, and then interpret $\vartheta' = 0$ and $\vartheta' = \pi$ not as points on a sphere but as circles on a cylinder. An example is shown in Fig. 6 where the two representations are compared. The top row exhibits S^\mp as in Fig. 4, the bottom row T^\mp . The north pole $(\vartheta, \psi) = (\pi/2, \pi/2)$ is transformed into the circle $\vartheta' = 0$ (upper boundary), and the south pole into the circle $\vartheta' = \pi$ (lower boundary). Identification of these circles between T^-

and T^+ produces the full torus T_2^2 on which the non-accessible white regions are now the two holes in the neighborhoods of the points $(\vartheta', \psi') = (\pi/2, 0)$ and $(\pi/2, \pi)$. Since corresponding boundaries $\partial\mathcal{U}_{h,l}$ on T^- and T^+ must also be identified, each pair of holes on the two sides generates a handle. Hence, the surface of section $\mathcal{P}_{h,l}^2$ for this example has the topology of a torus with two handles, i.e., it is a manifold M_3^2 . The lines of tangency, in this particular example, seem to have become lines of constant ϑ' .

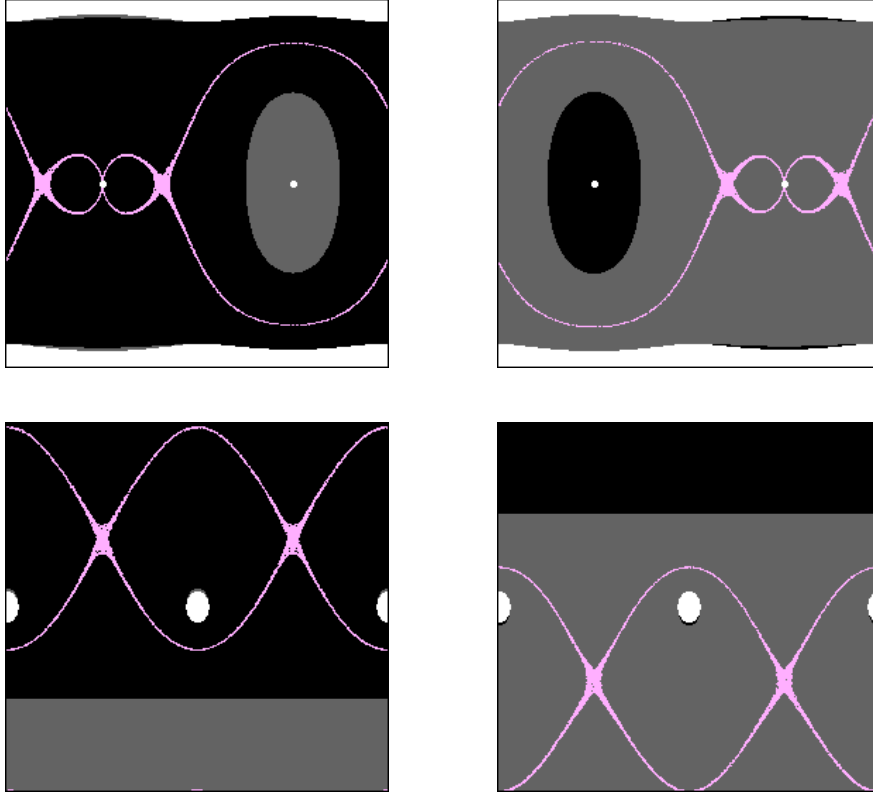


Figure 6: Comparison of the projection of $\mathcal{P}_{h,l}^2$ onto two copies S^\mp of the Poisson sphere $S^2(\vartheta, \psi)$ (top) and onto the two halves T^\mp of the torus $T_2^2(\vartheta', \psi')$ (bottom). The parameters are $A = (2, 1.5, 1)$, $\mathbf{r} = (1, 0, 0)$, $h = 80.5$, $l = 12.80$. Incoming intersections of the pink orbit are all on the left, outgoing on the right.

One trajectory has been added, in pink color. Its incoming part $\dot{S} < 0$ lies entirely on T^- , the outgoing part $\dot{S} > 0$ on T^+ . Note that the incoming

part of the trajectory comes close to the pole $\gamma = \hat{\mathbf{r}}$ whereas the outgoing part has points close to the south pole $\gamma = -\hat{\mathbf{r}}$. The comparison of upper and lower row illustrates that the torus T_2^2 is the most natural basis for a projection of $\mathcal{P}_{h,l}^2$.

Simpler manifolds occur, e. g., when $\mathcal{U}_{h,l}$ is a topological disk on $S^2(\gamma)$. If this disk does not include any of the poles $\pm\hat{\mathbf{r}}$, its representation on the PP-torus is two disks, one on each half. The surface of section is then the union of two disks which are glued together at their boundary; in other words, $\mathcal{P}_{h,l}^2$ is a topological sphere S^2 . If the disk contains just one of the poles, its representation on the torus is a cylinder, and $\mathcal{P}_{h,l}^2$ is the torus T^2 obtained by identifying its upper and lower rim. If both poles are contained in the disk, the same kind of arguments show that $\mathcal{P}_{h,l}^2$ is a 2-manifold of genus 2.

	Topology of a connected component of $\mathcal{E}_{h,l}^3$			
	\mathbb{RP}^3	S^3	$S^1 \times S^2$	$(S^1 \times S^2) \# (S^1 \times S^2)$
	Structure of $\mathcal{U}_{h,l}$			
\downarrow number of poles in $\mathcal{U}_{h,l}$	S^2	D^2	$S^2 \setminus 2D^2$	$S^2 \setminus 3D^2$
0	-	S^2	T^2	M_2^2
1	-	T^2	M_2^2	M_3^2
2	T^2	M_2^2	M_3^2	M_4^2

Table 1: Possible topologies of the Poincaré surface of section $\mathcal{P}_{h,l}^2$.

It is known from the work of Tatarinov [11] and Bolsinov et al. [2] that connected components of $\mathcal{U}_{h,l} \subseteq S^2(\gamma)$ come only in four topological kinds: the entire sphere S^2 , a disk $D^2 = S^2 \setminus D^2$, an annulus $S^2 \setminus 2D^2$, and a sphere with three holes $S^2 \setminus 3D^2$. The corresponding topological types of $\mathcal{P}_{h,l}^2$ are listed in Tab. 1, for all possible locations of the poles relative to $\mathcal{U}_{h,l}$. They are manifolds of genus g with g ranging from 0 to 4. If we distinguish pairs of $\mathcal{E}_{h,l}^3$ and $\mathcal{P}_{h,l}^2$ when either of the partners is different, then the table shows there are 10 different possibilities.

To wrap it up, we propose to start with the PP-torus $T_2^2(\vartheta', \psi')$ as the appropriate manifold onto which the Poincaré surface of section $\mathcal{P}_{h,l}^2$ is to be projected 1:1. It is constructed from two copies of the Poisson sphere where $+\hat{\mathbf{r}}$ serves as reference point for the polar coordinates (ϑ', ψ') . The spheres are punctuated at the two poles $+\hat{\mathbf{r}}$ and $-\hat{\mathbf{r}}$ which are replaced by circles

$(\vartheta', \psi') = (0, \psi')$ and (π, ψ') , respectively. Identifying corresponding circles on these two cylinders produces the torus. It will be seen in the next section that this identification involves a relative shift of the two angles ψ' by π . The PP-torus carries two copies of the accessible region $\mathcal{U}_{h,l}$. Boundaries $\partial\mathcal{U}_{h,l}$ of these two copies are to be identified. The resulting manifold is a 1:1 image of the complete Poincaré surface of section $\mathcal{P}_{h,l}^2$.

5 Examples

In this last section we give nontrivial examples of surfaces of section $\mathcal{P}_{h,l}^2$ where the extra bifurcation lines (13), or

$$h = \frac{l^2}{2\langle \hat{\mathbf{r}}, A\hat{\mathbf{r}} \rangle} \mp r, \quad (17)$$

do not coincide with bifurcations of the energy surface. This cannot happen in the Katok family of systems considered in [6] (which includes all cases of Lagrange and Kovalevskaya) because there the center of mass \mathbf{r} lies on a principal axis, and then (17) is the bifurcation line corresponding to the relative equilibrium where the body rotates about that axis. In order to make (17) different from any of the relative equilibrium conditions, we must choose \mathbf{r} off the principle axes. An arbitrary example is shown in Fig. 7, with $A = (2, 1.1, 1)$ and $\mathbf{r} = (0.94868, 0, 0.61623)$. The two orange lines separating from the red and blue relative equilibria correspond to $\gamma = \hat{\mathbf{r}}$ (left) and $\gamma = -\hat{\mathbf{r}}$ (right). When h is increased at fixed l , $\mathcal{U}_{h,l}$ is at first a disk which does not contain any of the poles. Upon crossing the left orange line, $+\hat{\mathbf{r}}$ enters $\mathcal{U}_{h,l}$, then at the right orange line, $-\hat{\mathbf{r}}$ comes in as well.

The six lines in Fig. 7 show a partition of the (h, l) -plane (with $l > 0$) into eight regions (plus the non-physical region to the left of the red line). Seven of them are represented by the black dots on the line $l = 3.25$. The tiny eighth region lies between the yellow and green lines to the left of the orange line (black dot at $(h, l) = (3.1486, 2.72)$). An additional region, not contained in the figure, exists because at large values of h and l the left branches of the yellow and orange lines intersect; point $(h, l) = (14.0, 7.2)$ is representative for this region where the left orange line lies to the right of the yellow line.

These nine regions correspond to nine different topologies of $\mathcal{P}_{h,l}^2$, including six of the types listed in Tab. 1, and three examples of disjoint surfaces of section. We discuss them one by one. The following Poincaré sections contain typical orbits, with different colors for different orbits. When certain

orbits are the same type (elliptic or hyperbolic) in different regions they are given the same color.

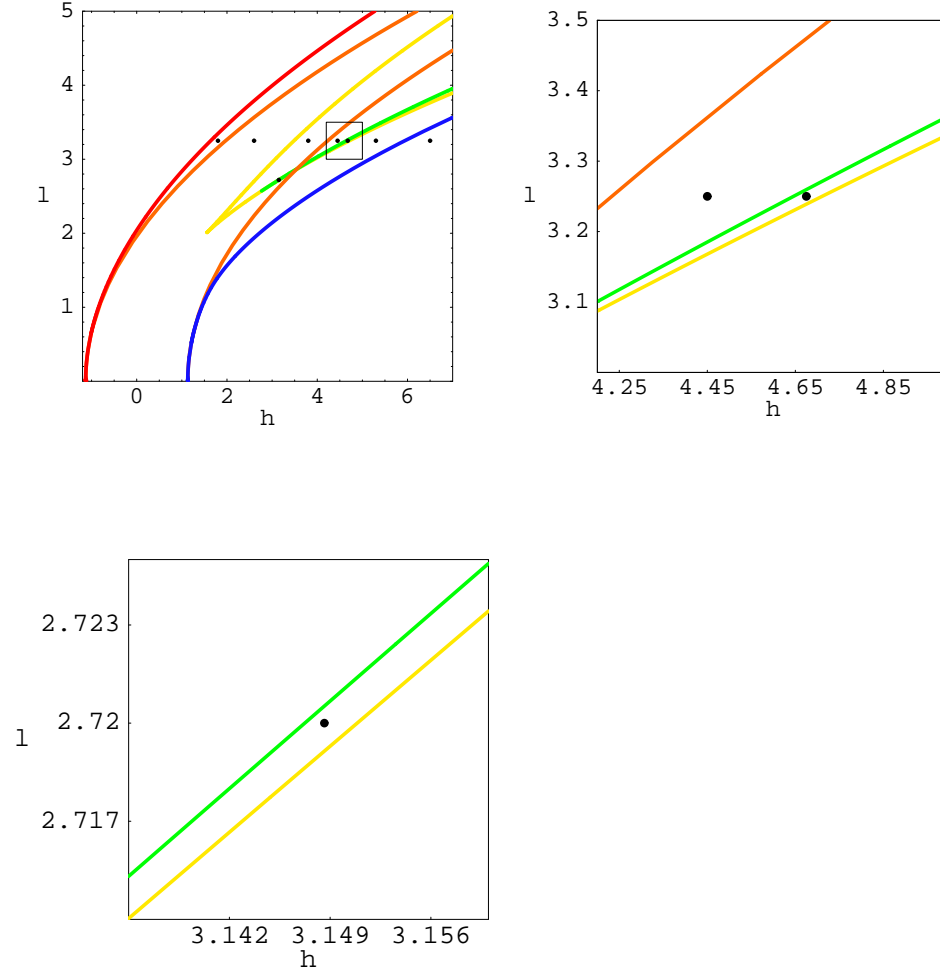


Figure 7: Bifurcation diagram for the Poincaré surface of section $\mathcal{P}_{h,l}^2$, for $A = (2, 1.1, 1)$ and $\mathbf{r} = (0.94868, 0, 0.61623)$. The red, blue, green, and yellow lines correspond to critical values of (7), the two orange lines come from (17). Top right: Magnification of the rectangle marked on the left. Bottom left: Magnification around the point $(h, l) = (3.1486, 2.72)$.

The first example $(h, l) = (1.8, 3.25)$ represents the leftmost region between the red and orange bifurcation lines. It is shown in the top row of

Fig. 8. The accessible region $\mathcal{U}_{h,l}$ on T^\mp is a rather small topological disk which does not contain the center of mass $\hat{\mathbf{r}}$. Gluing the two copies together along the boundary of $\mathcal{U}_{h,l}$ we obtain for $\mathcal{P}_{h,l}^2$ a topological sphere S^2 .

The second row of Fig. 8 shows the case $(h, l) = (2.6, 3.25)$. The north pole (upper rim) has entered $\mathcal{U}_{h,l}$. The orbit structure reveals that when we identify the two circles corresponding to $\hat{\mathbf{r}}$ on T^\mp , the angle ψ' must be shifted by π . On the Poisson sphere, $\mathcal{U}_{h,l}$ is again a disk D^2 , but on the torus $T^+ \cup T^-$ its two copies together form an annulus. Gluing together the two boundaries $\partial\mathcal{U}_{h,l}$ on T_2^2 we find that $\mathcal{P}_{h,l}^2$ is a torus T^2 .

Increasing the energy beyond the yellow line in Fig. 7, the topology of $\mathcal{E}_{h,l}^3$ changes from S^3 to $2S^3$, a new disjoint disk appears as part of $\mathcal{U}_{h,l}$. This disk contains no pole, hence we deduce that $\mathcal{P}_{h,l}^2$ is the union of a torus T^2 and a sphere S^2 , see the third row of Fig. 8 with $(h, l) = (3.8, 3.25)$. It may be surprising that the trajectories shown indicate only regular behavior with no sign of chaos even though the equations of motion are certainly non-integrable.

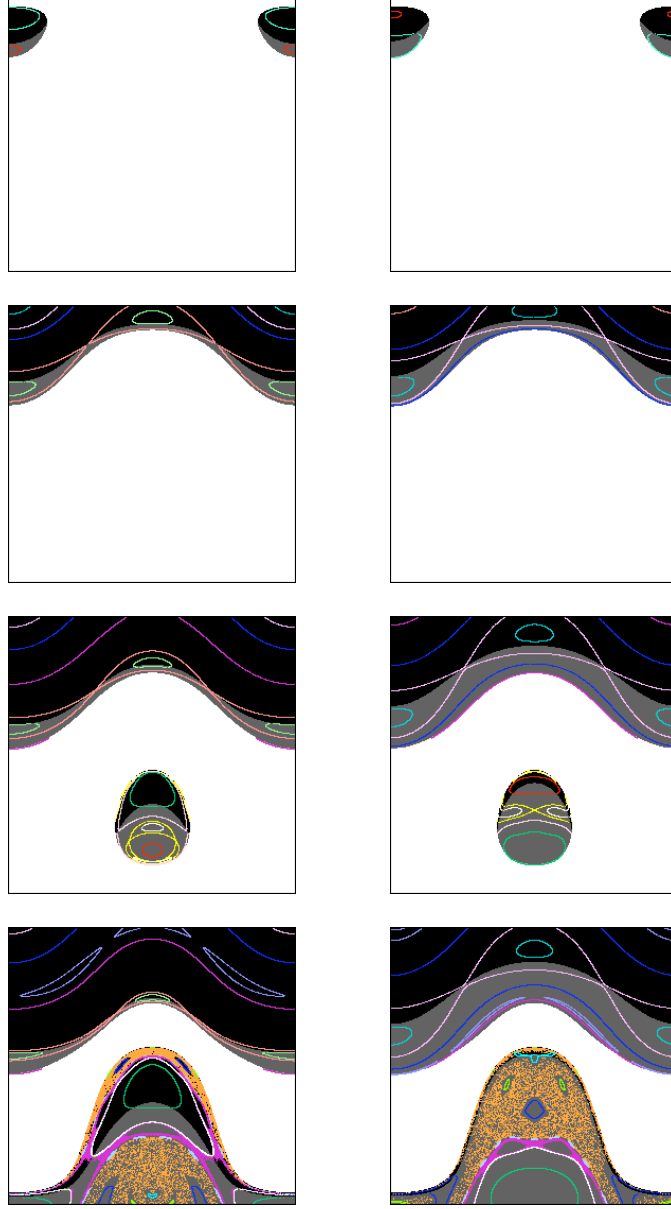


Figure 8: Projections of $\mathcal{P}_{h,l}^2$ onto T^- (left) and T^+ (right). Parameters are those of Fig. 7. The angular momentum is $l = 3.25$ for all cases, the energy from top to bottom is 1.8, 2.6, 3.8 and 4.45.

The next point $(h, l) = (4.45, 3.25)$, see the right part of Fig. 7 and the last row of Fig. 8, represents a region where both disjoint disks of $\mathcal{U}_{h,l}$ contain a pole. The surface of section is therefore $2T^2$. It appears that the accessibility of the south pole (corresponding to the center of mass in upright position) suddenly introduces manifest chaos. While the component around $\hat{\mathbf{r}}$ still looks very regular, the one containing $-\hat{\mathbf{r}}$ is dominated by chaotic motion. The orange and purple orbits belong to the same chaotic region but for a long time remain separate, indicating the presence of cantori related to the chain of islands between them.

The next three cases with $l = 3.25$ are shown in Fig. 9. The first row with $h = 4.675$ represents the narrow (h, l) -region between the green and yellow bifurcation lines, see the right part of Fig. 7. $\mathcal{U}_{h,l}$ is the Poisson sphere minus two disks, i. e., a topological annulus; as this annulus contains both poles, the surface of section $\mathcal{P}_{h,l}^2$ is a manifold M_3^2 of genus 3. Compared to the previous case $h = 4.45$, the two disks about the poles have merged at two points and now allow the chaos to sneak into the upper region. Nevertheless, the neighborhood of $\hat{\mathbf{r}}$ remains mostly regular.

One of the two inaccessible disks disappears as h is increased beyond the yellow line in Fig. 7, see the second row of Fig. 9 where $h = 5.3$. $\mathcal{U}_{h,l}$ is now a disk which contains both poles, hence $\mathcal{P}_{h,l}^2$ is a manifold M_2^2 of genus 2. It appears that the phase space is fairly distinctly divided into one chaotic and two regular parts. The “outgoing” intersections of the chaotic orbits take place in a region connected to the south pole $\hat{\mathbf{r}}$, the “incoming” lie between the poles. A bigger regular region surrounds the north pole, a smaller one connects to the south pole at about one half of the ψ' -circle. So chaos and order meet at the south pole, depending on the angle ψ' .

Finally, when h crosses the blue bifurcation line, the whole Poisson sphere becomes accessible. This is shown, with $h = 6.5$, in the last row of Fig. 9. The surface of section is now isomorphic to the entire PP-torus T_2^2 . As to the distribution of regular and chaotic orbits on this torus, we observe again two regular parts separated by two chaotic regions.

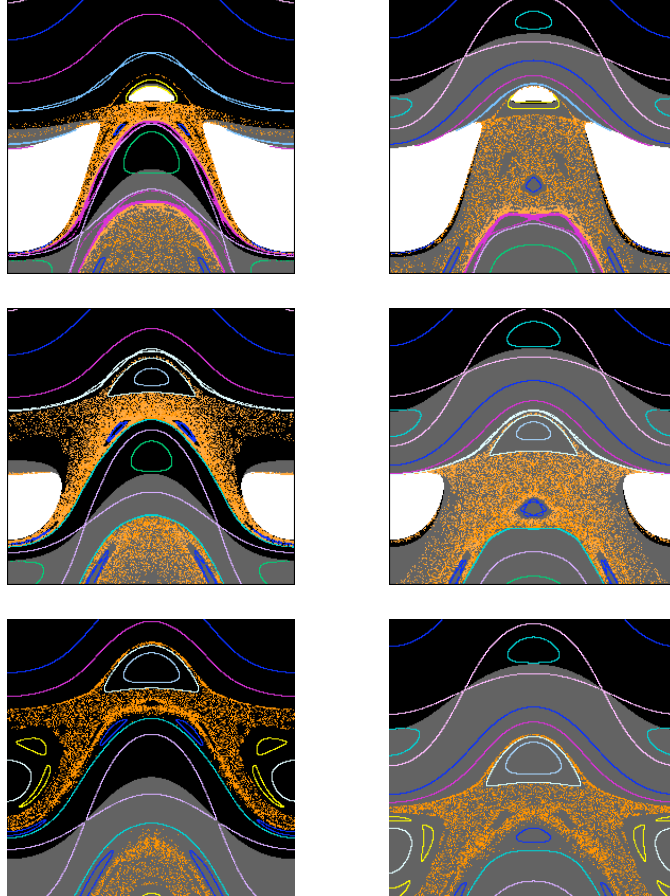


Figure 9: Projections like in Fig. 8. Again $l = 3.25$ in all three cases; the energy from top to bottom is 4.675, 5.3 and 6.5.

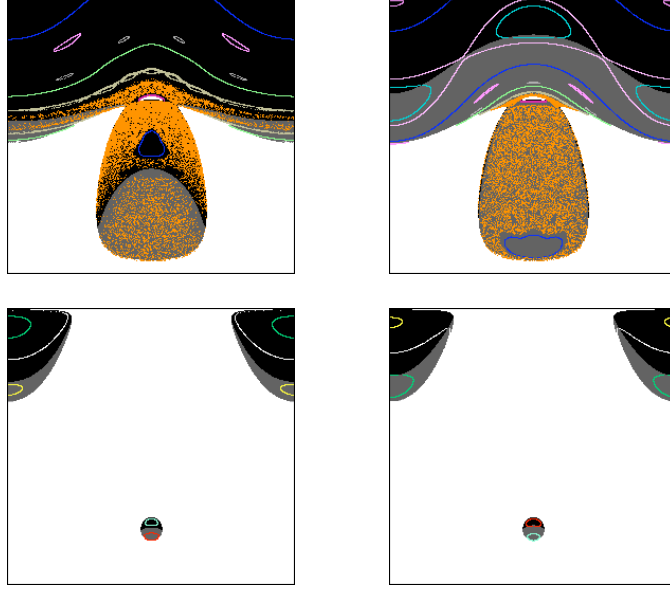


Figure 10: Projections of $\mathcal{P}_{h,l}^2$ like in Fig. 8. Top row $(h, l) = (3.1486, 2.72)$, bottom row $(14.0, 7.2)$ (bottom).

Two more types of surfaces of section are shown in Fig. 10. They do not exist for $l = 3.25$. The upper row shows the example $(h, l) = (3.1486, 2.72)$; the corresponding dot in Fig. 7 lies between the green and yellow lines, but to the left of the orange line. Compared to the first row of Fig. 9, the lower part does not contain the south pole, yet there remains a small hole (barely visible in the figure) inside the accessible region, near the center. $\mathcal{U}_{h,l}$ is a topological annulus containing the north pole, hence $\mathcal{P}_{h,l}^2$ is of type M_2^2 . In the scenario where this case emerges from the third row of Fig. 8, an outbreak of chaos takes place in the lower part.

The last case is $(h, l) = (14.0, 7.2)$; the accessible region consists of two disks neither of which contains a pole. Hence $\mathcal{P}_{h,l}^2$ is the union of two topological spheres.

With this series of nine types of $\mathcal{U}_{h,l}$ we have illustrated 6 out of the 10 possible topologies listed in Tab. 1. But notice that our choice $A = (2, 1.1, 1)$ represents only one of the seven different classes of moments of inertia that Katok distinguishes with $\hat{\mathbf{r}} = (1, 0, 0)$ (the class K2 in the notation of [6]). With other choices it is possible to also find examples for the other types of $\mathcal{U}_{h,l}$.

6 Summary and outlook

We have presented a new tool for the study of rigid body dynamics: a complete Poincaré surface of section $\mathcal{P}_{h,l}^2$ and its 1:1 representation in projection to a suitably defined torus, the PP-torus T_2^2 . The surface $\mathcal{P}_{h,l}^2 \subset \mathcal{E}_{h,l}^3$ is defined by local extrema of the vertical component of the center of mass \mathbf{r} , $d\langle\boldsymbol{\gamma}, \mathbf{r}\rangle/dt = 0$, and the PP-torus is obtained from two copies $S^+(\boldsymbol{\gamma})$ and $S^-(\boldsymbol{\gamma})$ of the Poisson sphere by the following procedure: punctuate $S^\pm(\boldsymbol{\gamma})$ at the points $\boldsymbol{\gamma} = \pm\mathbf{r}/r$, replace these points by “polar circles” to obtain two cylinders $T^\pm(\boldsymbol{\gamma})$, and then identify corresponding polar circles on $T^+(\boldsymbol{\gamma})$ and $T^-(\boldsymbol{\gamma})$. The torus T_2^2 so constructed contains two copies of the accessible $\boldsymbol{\gamma}$ -region, and $\mathcal{P}_{h,l}^2$ projects 1:1 to the union of these two copies. Identifying the boundaries $\partial\mathcal{U}_{h,l}$ on $T^+(\boldsymbol{\gamma})$ and $T^-(\boldsymbol{\gamma})$ produces a manifold which is homeomorphic to $\mathcal{P}_{h,l}^2$ and at the same time readily accessible to intuition.

We have shown examples for nine topologically different surfaces $\mathcal{P}_{h,l}^2$ and propose to use the tool for further exploration of the dynamics of rigid bodies in their 4-dimensional parameter space. In a forthcoming publication we will apply it to the family of systems $A = (2, 2\eta, 1)$, $\mathbf{r} = (1, 0, 0)$, which contains the integrable system of Lagrange ($\eta = 1$) and Kovalevskaya ($\eta = 2$). Pictures like those of Figs. 8-10 reveal the fate of particular features of the phase space structure under parameter variation, such as location and stability of isolated periodic orbits, their bifurcation schemes, as well as the extent and entanglement of regular and chaotic regions.

A Appendix: Explicit characterization of $\mathcal{P}_{h,l}^2$

Given an energy h , an angular momentum l , and a point $\boldsymbol{\gamma}$ on the Poisson sphere (not collinear with \mathbf{r}), we determine the corresponding vectors \mathbf{l} on the Poincaré surface defined by $S = 0$, or $\langle\mathbf{l}, A^{-1}(\mathbf{r} \times \boldsymbol{\gamma})\rangle = 0$. For abbreviation we introduce the notation

$$\mathbf{u} := A^{-1}(\mathbf{r} \times \boldsymbol{\gamma}), \quad \mathbf{v} := \mathbf{u} \times \boldsymbol{\gamma}. \quad (\text{A.1})$$

The equations $S = \langle \mathbf{l}, \mathbf{u} \rangle = 0$ and $L = \langle \mathbf{l}, \boldsymbol{\gamma} \rangle = l$ define planes in \mathbf{l} -space which intersect in a line with direction \mathbf{v} . It is easy to check that

$$\mathbf{l}_0 = l \frac{\mathbf{v} \times \mathbf{u}}{\langle \mathbf{v}, \mathbf{v} \rangle} \quad (\text{A.2})$$

is one point on this line, hence we may parameterize it with $\mathbf{l} = \mathbf{l}_0 + \mathbf{v}t$. The energy equation (3) determines the possible values of t . We write it in the form

$$\langle \mathbf{l}_0 + \mathbf{v}t, A^{-1}(\mathbf{l}_0 + \mathbf{v}t) \rangle = 2(h + \langle \mathbf{r}, \boldsymbol{\gamma} \rangle) =: c. \quad (\text{A.3})$$

This gives a quadratic equation for t ,

$$\langle \mathbf{v}, A^{-1}\mathbf{v} \rangle t^2 + 2\langle \mathbf{l}_0, A^{-1}\mathbf{v} \rangle t + \langle \mathbf{l}_0, A^{-1}\mathbf{l}_0 \rangle - c = 0. \quad (\text{A.4})$$

Inserting its solutions into $\mathbf{l} = \mathbf{l}_0 + \mathbf{v}t$, we find $\mathbf{l} = \mathbf{l}_1 \pm \mathbf{l}_2$ with

$$\mathbf{l}_1 = \mathbf{l}_0 - \frac{\langle \mathbf{l}_0, A^{-1}\mathbf{v} \rangle}{\langle \mathbf{v}, A^{-1}\mathbf{v} \rangle} \mathbf{v} \quad (\text{A.5})$$

and

$$\mathbf{l}_2 = \frac{\mathbf{v}}{\langle \mathbf{v}, A^{-1}\mathbf{v} \rangle} \sqrt{\langle \mathbf{l}_0, A^{-1}\mathbf{v} \rangle^2 - (\langle \mathbf{l}_0, A^{-1}\mathbf{l}_0 \rangle - c)\langle \mathbf{v}, A^{-1}\mathbf{v} \rangle}. \quad (\text{A.6})$$

To evaluate further, we use an identity which holds for arbitrary symmetric matrices A and vectors \mathbf{a}, \mathbf{b} :

$$A\mathbf{a} \times A\mathbf{b} = (\det A) A^{-1}(\mathbf{a} \times \mathbf{b}). \quad (\text{A.7})$$

For example, with $\mathbf{v} = \mathbf{u} \times \boldsymbol{\gamma}$ we find $A^{-1}\mathbf{v} = (A\mathbf{u} \times A\boldsymbol{\gamma})/\det A$ and

$$\langle \mathbf{v}, A^{-1}\mathbf{v} \rangle = \frac{1}{\det A} \langle \mathbf{u} \times \boldsymbol{\gamma}, A\mathbf{u} \times A\boldsymbol{\gamma} \rangle = \frac{1}{\det A} \langle \mathbf{u}, A\mathbf{u} \rangle \langle \boldsymbol{\gamma}, A\boldsymbol{\gamma} \rangle; \quad (\text{A.8})$$

in the last step we used Lagrange's identity and $\langle \boldsymbol{\gamma}, A\mathbf{u} \rangle = \langle \boldsymbol{\gamma}, \mathbf{r} \times \boldsymbol{\gamma} \rangle = 0$. With similar arguments, and using the explicit form (A.2) for \mathbf{l}_0 , we find

$$\mathbf{l}_1 = l \frac{A\boldsymbol{\gamma}}{\langle \boldsymbol{\gamma}, A\boldsymbol{\gamma} \rangle}. \quad (\text{A.9})$$

To evaluate \mathbf{l}_2 , we first employ Lagrange's identity to obtain

$$\langle \mathbf{l}_0, A^{-1}\mathbf{v} \rangle^2 - \langle \mathbf{l}_0, A^{-1}\mathbf{l}_0 \rangle \langle \mathbf{v}, A^{-1}\mathbf{v} \rangle = \langle \mathbf{l}_0 \times \mathbf{v}, A^{-1}\mathbf{v} \times A^{-1}\mathbf{l}_0 \rangle, \quad (\text{A.10})$$

and then (A.7) with A^{-1} instead of A to transform this into

$$\frac{-1}{\det A} \langle \mathbf{l}_0 \times \mathbf{v}, A(\mathbf{l}_0 \times \mathbf{v}) \rangle. \quad (\text{A.11})$$

An easy calculation using $\langle \mathbf{v}, \mathbf{u} \rangle = 0$ shows that $\mathbf{l}_0 \times \mathbf{v} = l\mathbf{u}$. Inserting this into the radicand of (A.6) we find that it may be written as

$$\frac{\langle \mathbf{u}, A\mathbf{u} \rangle}{\det A} (c\langle \gamma, A\gamma \rangle - l^2) = 2\langle \mathbf{v}, A^{-1}\mathbf{v} \rangle (h - U_l(\gamma)) \quad (\text{A.12})$$

with the effective potential of Eq. (5). The final result for l is

$$l = l \frac{A\gamma}{\langle \gamma, A\gamma \rangle} \pm \mathbf{v} \sqrt{\frac{2(h - U_l(\gamma))}{\langle \mathbf{v}, A^{-1}\mathbf{v} \rangle}}. \quad (\text{A.13})$$

Acknowledgements

We thank Igor Gashenko for many discussions.

References

- [1] V. I. Arnold. *Mathematical Methods of Classical Mechanics*, volume 60 of *Graduate Texts in Mathematics*. Springer, Berlin, Heidelberg, New York, 1978.
- [2] A. Bolsinov, H. R. Dullin, and A. Wittek. Topology of energy surfaces and existence of transversal Poincaré sections. *J. Phys. A*, 29:4977–4985, 1996.
- [3] H. R. Dullin. *Die Energieflächen des Kowalewskaja-Kreisels*. Mainz Verlag, Aachen, 1994.
- [4] H. R. Dullin, M. Juhnke, and P. H. Richter. Action integrals and energy surfaces of the Kovalevskaya top. *Int. J. Bifurcation and Chaos*, 4(6):1535–1562, 1994.
- [5] H. R. Dullin and A. Wittek. Complete Poincaré sections and tangent sets. *J. Phys. A*, 28:7157–7180, 1995.
- [6] I. N. Gashenko and P. H. Richter. Enveloping surfaces and admissible velocities of heavy rigid bodies. *Int. J. Bifurcation and Chaos*, 14(8):2525–2553, 2004.

- [7] S. B. Katok. Bifurcation sets and integral manifolds in the problem of motion of a heavy rigid body. *Usp. Math. Nauk*, 27:126–132, 1972.
- [8] P. H. Richter. Regular and chaotic rigid body dynamics. *Nonlinear phenomena in complex systems*, 9(2):115–124, 2006.
- [9] P. H. Richter, H. R. Dullin, and A. Wittek. Kovalevskaya Top. *Publikationen zu Wissenschaftlichen Filmen, Sektion Technische Wissenschaften/Naturwissenschaften*, 13:33–96, 1997. Film C1961, Institut für den Wissenschaftlichen Film (IWF), Göttingen.
- [10] Ya. V. Tatarinov. On the study of the phase space topology of compact configurations with symmetry. *Vestnik Moskov. Univ., Ser. Math.-Mekh.*, 5:70–77, 1973.
- [11] Ya. V. Tatarinov. Portraits of classical integrals in the problem on rotation of a rigid body about a fixed point. *Vestnik Moskov. Univ., Ser. Math.-Mekh.*, 6:99–105, 1974.